Indian Journal of Fibre & Textile Research
Vol. 51, March 2026, pp. 74-83
DOI: 10.56042/ijftr.v51i1.5869

Rayon-based activated carbon fabric with controlled porosity: advanced barrier against chemical warfare agents (CWAs)

Manish Kr Singh[1,2], J P Singh[1,a], Harish Chandra Joshi[2], Rohitashaw Kr Singh[2], Uttam Saha[2] & Mayank Dwivedi[2]

[1]Department of Textile Technology, Uttar Pradesh Textile Technology Institute, Kanpur 208 001, India

[2]Technical Textile Division, Defence Material and Store Research and Development Establishment, Kanpur 208 013, India

Received 27 September 2023; revised received and accepted 11 July 2024

Currently, activated carbon fibre (ACF) is a material of choice for various adsorption applications, offering numerous advantages over conventional forms of activated carbon, such as powders and beads. Among the possible precursors for ACF-like pitch, PAN, and phenol, rayon is relatively cheaper and abundantly commercially available. We report here the preparation of ACF from a commercially available rayon-based carbon fabric via gasification in a CO_2 atmosphere. A series of four samples was prepared by varying activation time (4 h, 4.5 h, and 5 h) and temperature (850 °C, 900 °C & 950 °C) at a constant CO_2 flow rate of 100 ml/min. The prepared ACFs were assessed for Brunauer-Emmett-Teller (BET) surface area, distribution of pores, and adsorption isotherms. Further, activated carbon was investigated using X-ray diffraction and field-emission scanning electron microscopy. The chemical environment of the carbonized & ACF samples has been assessed through FTIR. The evaluation of fabric properties in terms of mass, bending length, and flexural rigidity for carbonized fabric and ACF was also carried out. The prepared ACFs show a well-developed porous structure and activated carbon in a self-supporting textile form. The optimum activation conditions were obtained for ACF prepared at 900 °C for an activation duration of 4 h in CO_2 with a flow rate of 100 ml/min. The material is predominantly microporous and suitable for the adsorption of hazardous chemicals. The prepared ACF may find many usages in different adsorptional applications for the removal of toxic gases and as an adsorbent medium against lethal chemical warfare agents in military clothing systems.

Keywords: ACF, Adsorption, Gas flow rate, Micro porous, Surface area, Time & temperature

1 Introduction

Activated carbon in the form of beads, pellets, and granules has been widely prepared from various precursors and explored for different adsorptional applications. Among the various forms of activated carbon, activated carbon fabric (ACF) is known to be an advanced form of porous carbon available in self-supporting textile form with numerous advantages over conventional forms of activated carbon[1-3]. The main advantages of ACF are-

i) Higher adsorption rate due to finer fiber count, which minimizes mass transfer limitations.
ii) Homogeneous distribution of pore size along with excellent adsorption capacity at lower concentration.
iii) The fibres may be configured in various physical forms like felt, fabrics, and nonwoven.
iv) Activated carbon fabric is used in many applications, like antibacterial wound dressings, disposable gas masks, gas storage, electrodes for capacitors, and in military chemical protective clothing.

Irrespective of physical form, any organic material with high carbon content and thermosetting properties can be converted into porous carbons by thermal treatment in a suitable gasifying atmosphere. The activated carbon is synthesized through two main steps: (i) carbonization and (ii) activation, as shown in Fig. 1. ACFs are prepared by pyrolyzing textile polymeric precursors like pitch[4,5], pan[6-8], phenol[9-11] and rayon[12-14] for conversion into carbon fabric. Some precursors, such as pitch- and PAN-based precursors, undergo an additional stabilization step before carbonization. The carbonization of the precursor is carried out in an inert atmosphere in the temperature range of 800-1000 °C, whereas the activation of the carbonized product is carried out in an oxidizing atmosphere, viz., in the presence of carbon dioxide, steam, or a mixture of both[15-17].

A simple carbonization process does not produce materials with adequate adsorption capacity owing to their less developed pores and low surface area. The pore structures formed during carbonization are

[a]Corresponding author.
E-mail: jpsingh.iitd@gmail.com

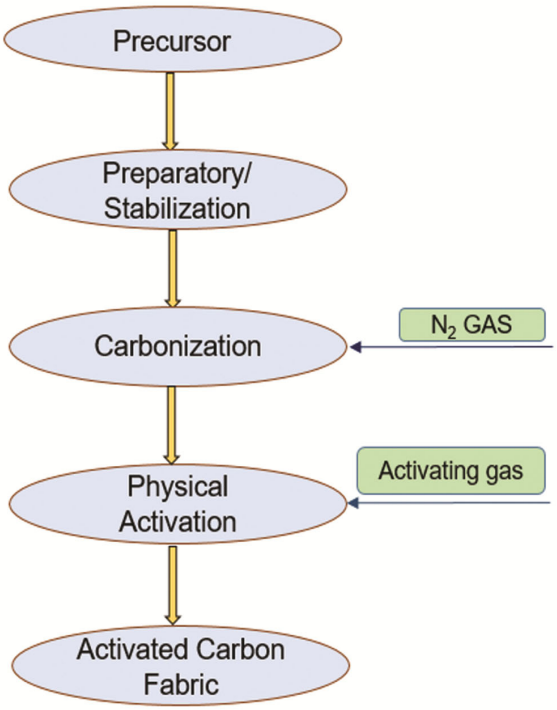

Fig. 1 — Schematic of preparation of ACF

further enhanced during activation. The activation process converts the carbonized material into a form that contains the highest number of randomly distributed pores of various sizes and shapes, thereby giving the product an extended, extremely high surface area. According to IUPAC norms, the porosity generated in activated carbon is defined on the basis of the size of pores as (a) micro pores (width less than 2 nm), (b) meso pores (width 2 to 50 nm), and (c) macro pores width greater than 50 nm[18].

When a gas or liquid is brought into contact with the porous solid phase, the gas/liquid, or some of its constituents, is concentrated on the surface due to unsaturated valences and weak molecular forces at the surface[19]. This phenomenon is called adsorption, and the solid being used to adsorb gases or liquid adsorbates is called an adsorbent. In general, silica gel, activated alumina, zeolites and activated carbons are used as adsorbent materials[20].

Total surface area & pore size distribution in activated carbon depends on various factors like nature of initial precursor, history of carbonization, nature of activating gas, heating rate, reactor design and various processing parameters of activation viz. time, temperature and flow rate of activating agent[21]. Pore-size distribution in activated carbon (Activated carbon fabric in our study) is an important factor, given its application. Highly microporous activated carbon fabric is desired for adsorption applications in gaseous-contaminated atmospheres, whereas mesoporous carbon is used for the adsorption of large molecules in liquid-phase adsorption. Activated carbon is hydrophobic, enabling its use in open environments under all weather conditions. Activated carbon is one of the strongest and unique adsorbents known to mankind due to its high surface area and microporous nature[22]. Such active carbons are known to be very good adsorbents for blistering and nerve agents at room temperature and play a major role in chemical protective clothing like nuclear, biological, chemical (NBC) suits[23-26]. NBC suits require high-surface-area activated carbon with a narrow pore-size distribution & adequate strength. This is achieved by selecting a suitable precursor and optimizing processing parameters. In the present study, the effect of processing conditions for the preparation of ACF from rayon fabric (carbon) is reported. The characterizations of the prepared ACF indicate a high surface area, microporous carbon, and good mechanical strength and flexibility. It could be used as an excellent adsorbent material in different applications, right from military clothing to commercial uses[27,28].

2 Materials and Methods

2.1 Materials

Commercially available rayon-based carbon fabric (320 gsm) in a satin weave was used as a precursor for ACF preparation. The satin weave fabric had 52 ends and 52 picks per inch. Carbon dioxide and N_2 gases were procured locally and passed through a series of adsorbents to remove moisture and any organic impurities.

2.2 Process of Activation

7.5 x 14 cm rayon-based carbon fabric was hung inside a vertical tubular furnace as shown in Fig. 2. The furnace had a quartz tubular reactor with an internal diameter of 10 cm. The furnace was equipped with appropriate arrangements for the passage of CO_2 and N_2 gases to ensure a constant flow of gas from the bottom of the reactor. The uniform heating zone inside the reactor was accurately measured using a Chrome/Alumel thermocouple before conducting experiments. Fabric strips were placed in the reactor's uniform heating zone to avoid thermal gradients. The temperature was controlled with a microprocessor-based programmable temperature controller (PID).

Activation or physical gasification was carried out in a CO_2 gaseous environment by varying time durations (4 h to 5 h) and temperature (850 °C to 950 °C) under a constant flow rate of 100 ml/min of activating gas. In all experiments, a constant heating rate of ~10 °C was maintained from room temperature to the desired activation temperature. Samples were placed inside the reactor and heated from room temperature to the desired activation temperature under an inert gas flow. Once the desired activation temperature was reached, the inert gas was turned off, and CO_2 gas was passed for different time durations. After activation was complete, the CO_2 gas was turned off, and the samples were cooled to room or ambient temperature under an inert gas atmosphere before being removed from the furnace.

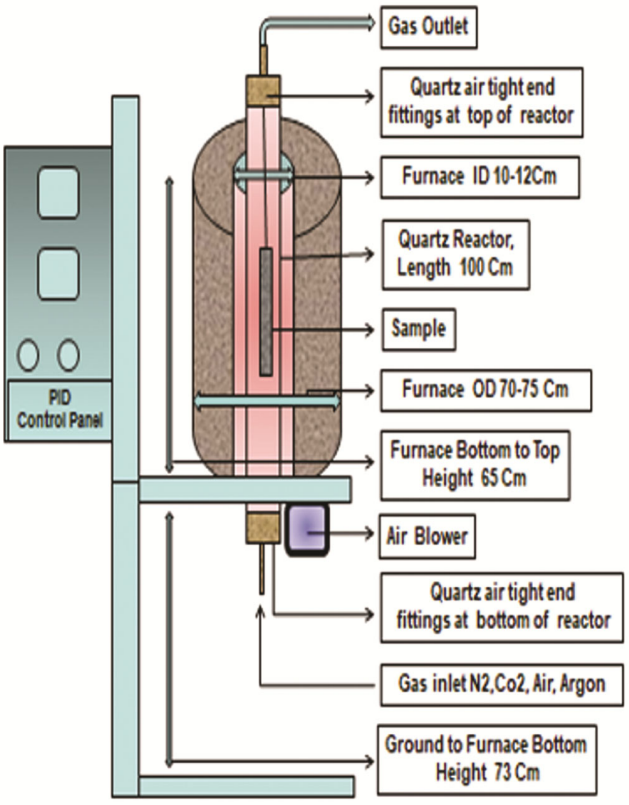

Fig. 2 — Schematic of tubular furnace

2.3 Brunauer-Emmett-Teller Surface Area and Porosity Measurement

An Autosorb C-1 BET surface area analyser (Anton Par, USA) was used for measurement of BET surface area, micro pore volume, total pore volume, and average pore width. The instrument is coupled with a data processor to measure BET surface area and pore volume. The surface area evaluation is based on the BET theory using N_2 gas as an adsorbate on ACF samples at 77K (-196 °C). Pore volume is measured from nitrogen adsorption isotherms at 77K on ACF samples at a relative pressure of close to unity (0.99994).

3 Results & Discussion

3.1 BET Surface Area and Pore Size Distribution

Several experiments were conducted on rayon-based carbon fabric, varying process parameters to examine their effects on surface properties and porosity development. The activation conditions and test results for four representative samples (RSM-1, 3, 5 & 7) are summarized in Table 1.

It is evident from Table 1 that all samples prepared (RSM-1, 3, 5 & 7) have a high surface area with a well-developed porous structure. It is observed that by varying processing conditions (time and temperature), BET surface area could be varied from 870 m^2/g (sample RSM-1) to as high as 2533m^2/g (sample RSM-3). Table 1 indicates that, at a constant CO_2 flow rate, the burn-off value in the samples is strongly affected by both time and temperature. The experimental results reveal that a surface area of ~870.32 m2/g (sample RSM-1) is obtained at 850 °C after 4.5 h of activation. Further, surface area is substantially increased to 2533 m^2/g at 950 °C for the same duration of activation time (sample RSM-3). Micro pore volume and total pore volume are also significantly increased from 0.32 cc/g to 0.83cc/g and from 0.37 cc/g to 1.56 cc/g, respectively. The average pore diameter is increased from 17 Å to 24 Å. The burn-off value increases significantly from ~22 % to 87 %.

Table 1 — Shows the surface area, pore volume and burn off percentage of ACF

Sample	Flow rate, ml/min	Temp, °C	Time, h	Burn off, %	BET surface area, m^2/g	Micro pore volume, cc/g	Total pore volume, cc/g	Avg. pore dia, Å
RSM-1	100	850	4.5	22.2	870.32	0.32	0.37	17.2
RSM-3	100	950	4.5	87.1	2533.33	0.83	1.56	24
RSM-5	100	900	4.0	46.4	1544.23	0.56	0.71	18.5
RSM-7	100	900	5.0	48.2	1318.76	0.48	0.60	18.3

Table 1 shows that sample RSM-1 is a highly microporous ACF with an initial burn-off value of ~22 %. This burn off is primarily responsible for the initial stage of porosity development. In the initial stage of activation, a large number of micropores are created through the controlled reaction of CO_2 with the carbon fabric. It is observed that an increase in temperature from 850 ℃ to 900 ℃ has led to a significant increase in burn-off value from ~22 % to ~46 %. This has increased the BET surface area from 870.32 m^2/g to 1544.23 m^2/g accordingly. From this data, it can be inferred that temperature has a marked influence on the formation of a large number of micro pores, with a shorter activation duration of 4 h at 900 ℃ compared to 4.5 h at 850 ℃. Accordingly, micro pore volume and total pore volume are increased from 0.32 cc/g to 0.56 cc/g and from 0.37 cc/g to 0.71 cc/g, respectively. In these results, burn-off primarily contributes to the creation of internal porosity, as evident from the BET and micro-pore volume data.

Table 1 indicates that samples RSM-5 and RSM-7 are prepared under identical conditions of flow rate (100 ml/min) and temperature (900 ℃), except for the increased activation duration from 4 h to 5 h. Sample RSM-7 has shown a moderate decrease in BET surface area, micro pore volume, and total pore volume. A possible explanation for this result could be based on the mechanism of porosity development in the material during the gasification process. During the process, amorphous carbon in the carbonized fabric may initially react with CO_2 to open blocked pores, and burning of carbon from exposed aromatic sheet/crystalline regions may also occur simultaneously, leading to the formation of new micro pores. Further activation for longer durations may lead to a reduction in micro-pore volume due to burning off carbon between the walls of two neighbouring micro-pores. In this case, most of the micro-pores are lost. This ultimately leads to decreases in micro-pore volume, adsorption capacity, and material mechanical strength. Further, this phenomenon is also supported in literature as reported by Kim K. W *et al.*[29].

Finally, sample RSM-3 was prepared at the highest activation temperature of 950 ℃ for 4.5 h, using the same flow rate. Under similar conditions of activation duration (4.5 h) for samples RSM-1 & 3, it is observed that the BET surface area, pore volume, and burn-off value are increased to a large extent in sample RSM-3. It is brought out here that the mechanical strength of sample RSM-3 was found to be very poor. The above results and findings observed in ACF samples could be explained in terms of porosity development stages and mechanisms. Activation is the process of creating new pores and cleaning blocked pores in a carbonized material. The gasification reaction of CO_2 during the activation process is a controlled oxidation reaction. This oxidation is a complex process comprising the transport of CO_2 to the carbon surface, diffusion within pores, reaction with carbon, desorption of reaction products, and diffusion of these products back to the carbon surface. Temperature, along with other activation parameters (activation duration and CO_2 flow), plays a major role during the entire process.

During the activation process, firstly, disorganized amorphous carbon is eliminated, opening closed porosity, followed by the burning of carbon from the exposed aromatic sheets. The extent of burn-off describes the degree of activation and the formation of porosity. This happens initially and linearly with temperature when burn-off is low. Following the burning of amorphous carbon, carbon from active and aromatic sheets begins to burn, leading to the formation of new pores and, later, the widening of the porosity. Further, extensive activation leads to high weight loss, increasing meso- and macro-pores. During the process, the neighbouring walls of two pores are burnt, leading to the conversion of micro pores into wider mesopores. Hence, this implies that the micro-pore volume contribution is decreased, and, as a result, there is no significant increase in adsorption capacity or internal surface area**.**

3.2 N_2 Adsorption Isotherm Studies on ACFs at 77K (-196 ℃)

N_2 Adsorption isotherms are fingerprints for any activated carbon material, which describe porosity development stages under different conditions. The formation of pores and their size distribution in ACF may be explained by the shapes of N_2 adsorption isotherms on activated carbon fabric at 77K. The adsorption isotherms have been classified into four groups according to the BDDT (Brunauer-Deming-Deming-Teller) classification[30]. The adsorption/ desorption isotherm of four representative samples, as described in Table 1 are represented in Fig. 3.

3.3 Effect of Time and Temperature on Activated Carbon Samples

The shape of the curve for RSM-1, ACF sample, shows a Type-1 isotherm, characteristic of microporous

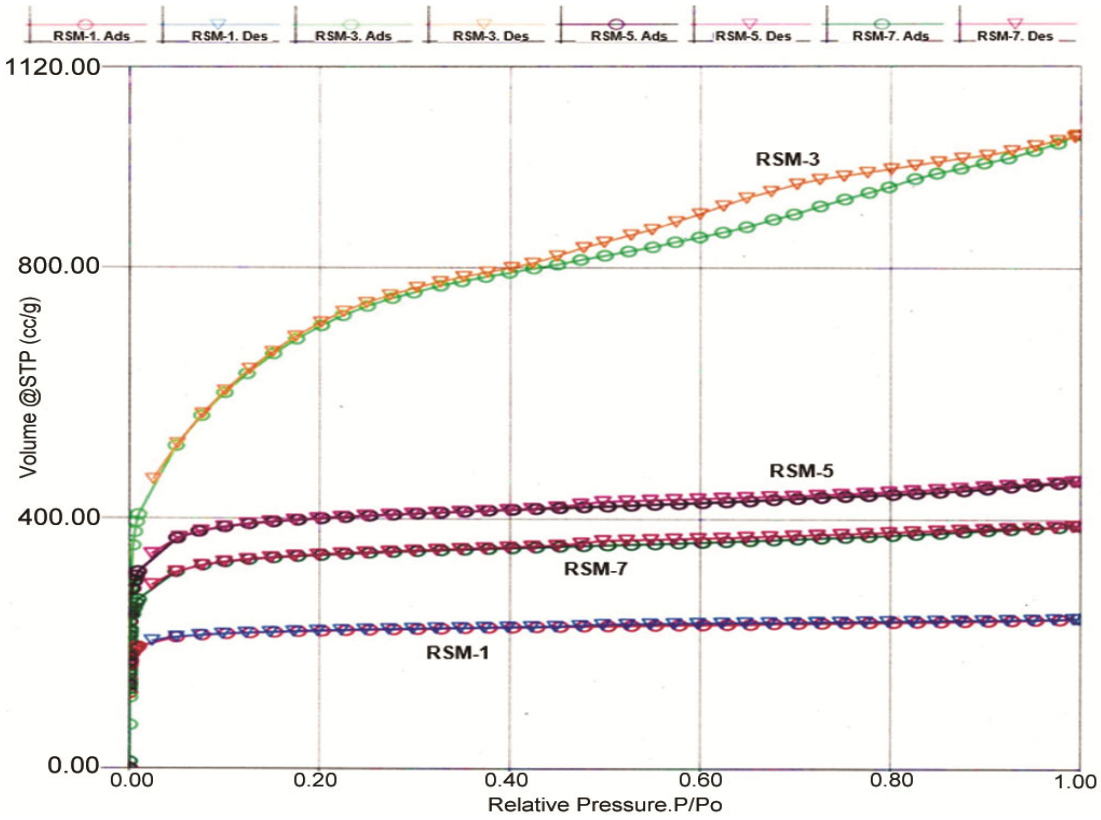

Fig. 3 — Adsorption/Desorption Nitrogen Isotherm of ACF at 77K

carbon according to the BDDT classification. It can be seen from the isotherm that there is a large volume uptake initially at lower relative pressures ($p/p_0 < 0.1$) and further, no uptake is observed[31]. This reflects a narrow-porosity material formed during the initial stages of porosity development, as discussed in section 3.1. In such microporous materials, the adsorption process is complete at a relative pressure below 0.5 ($p/p_0 < 0.5$). This feature suggests a uniform, narrow pore-size distribution, consistent with a micro-pore-filling phenomenon[32]. In such cases, surface area and pore volume is mainly contributed by micro pores. This is also reflected in the low burn-off value obtained for the sample as given in Table 1. The low burn-off suggests that the activation reaction of CO_2 with the carbon surface has created a large number of micro-pores as the initial step, where disordered carbon is released from closed pores, and new micro-pores are also formed by the exposure of aromatic sheets to CO_2.

In a similar manner, samples (RSM-5 & 7) were prepared under identical conditions of temperature (900 °C) and CO_2 flow rate (100 ml/min), with activation durations of 4 h and 5 h, respectively. As shown in Fig. 2, both samples exhibit similar isotherm shapes. For both samples, the isotherm shows a rounded knee below p/p_0 ~0.1, and thereafter the curve becomes almost horizontal with respect to the X-axis. Both samples are again of a typical micro-porous nature, similar to sample RSM-1. As discussed in section 3.1, the micro-pore volume, total pore volume, and surface area are marginally decreased for sample RSM-7. This could be explained in terms of the material's porosity development stages. Table 1 indicates that the RSM-5 sample exhibits a reasonable surface area and micropore volume when the carbon fabric is activated at 900 °C for 4 h. As discussed under section 3.1, increasing the activation time from 4 h to 5 h may have helped widen the existing micro pores by burning off carbon between the neighbouring walls of two connected micro pores.

The sample (RSM-3) shows a Type-IV isotherm, typical of mesoporous carbon. Such isotherms exhibit significant hysteresis, indicating that the desorption path does not follow the adsorption path. This hysteresis may be associated with capillary condensation in wider mesopores[33]. In such samples, the pore-size distribution is broader, with significant mesopore formation. The isotherm shows a small

volume uptake at lower relative pressures, which increases further at higher relative pressures. There is continuous volume uptake above p/p_0 ~0.1, and the adsorption process is incomplete below p/p0 ~0.5, suggesting that the material is heterogeneous, consisting predominantly of mesopores and micro pores. Moreover, the indication of a hysteresis loop, i.e., irreversible isotherms, clearly indicates the mesoporous nature of ACF. This shape is consistent with the surface characteristics given in Table 1. Although the surface area is high, the sample's mechanical strength was very low. Also, the high burn-off value indicates that some external gasification might have also occurred. This might be one of the reasons for the low mechanical strength observed.

3.4 Fourier Transform Infrared (FTIR) Analysis

ATR FT-IR measurements were carried out on carbon & ACF samples using a Bruker Tensor 27 (Bruker, Germany) equipped with Diamond crystal-based ATR. All spectral data were recorded at a resolution of 4 cm^{-1} and with 8 scans over the range of 4000 cm^{-1} to 650 cm^{-1}. FT-IR spectra of ACF showed four major absorption bands at ~3748 cm^{-1}, 2364 cm^{-1}, 1475 cm^{-1} & 682 cm^{-1} (Fig. 4). The bands in the

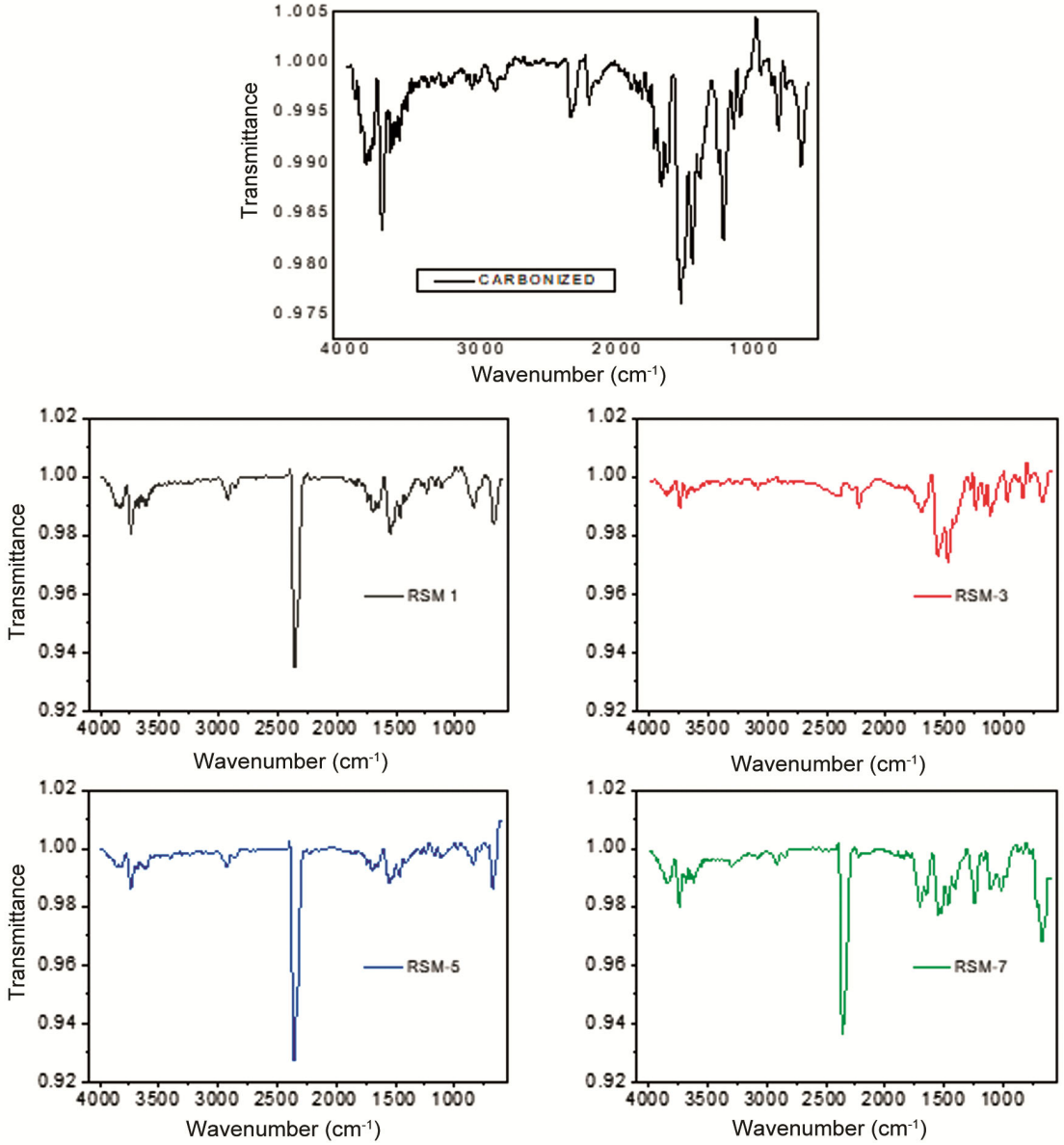

Fig. 4 — Fourier transform infrared spectroscopy analysis of different samples

region of 3748 cm^{-1} are assigned to the O–H stretching vibration and show the presence of free hydroxyl groups on the surface[34]. A strong peak is observed at ~2364 cm^{-1} in the ACF sample RSM 1, 5, and 7, except RSM 3. This strong peak is assigned to carbon dioxide contamination [CO_2] due to the activation process[35].

The peak intensity is low in the carbonized fabric, but it increases in ACF samples, confirming that CO_2 is incorporated during the activation process. This peak can also be related to the C≡C stretching vibration in ACF. The bands at 1475 cm^{-1} indicate the bending vibrations of the C-H group and confirm the presence of lignin[36]. Moreover, the absorption peak at 682 cm^{-1} is attributed to –C=C bending in the as-synthesized activated carbon.

3.5 FESEM Analysis

Field emission scanning electron microscopy of carbonized and activated rayon fabric at various activation conditions has been investigated, and it was found that the SEM image of carbonized fabric (10 KX), as shown in Fig. 5 (a), has a smooth surface without any perforation or cavities, and the diameter of the carbonized fibre is 6.65µm. Fibre surface for sample RSM-1 at 200 KX magnification shows small pits (~30-50 nm) and surface roughening, suggestive of a gasification reaction, as shown in Fig. 5 (b). However, cavities and pits are not very visible at lower (25 KX) magnification, as shown in Fig. 5 (c). The SEM image of sample RSM-3 (Temp. – 950 °C, time - 4.5 h & burn off – 87 %) is shown in Fig. 5 (d) at 100 KX. The SEM images in Fig. 5 (d) show extensive gasification of CO_2 at the fibre surface. This is also reflected by the high burn-off value obtained for the sample. The image reveals widening of cracks or cavities on the surface, leading to damage to the fibre surface. On physical inspection, the sample was found to be weak and fragile, despite the very high surface area obtained.

From the test data shown in Table 1, the samples RSM-5 & 7, with adequate strength and suitable BET surface area, may be used for practical applications in chemical protective clothing. The SEM Images for samples 5 & 7 are shown in Fig. 5 (e) & 5 (f), respectively. As compared to the fibre surface as observed in sample RSM-3, the fibre surface is not deteriorated largely, and the appearance of small

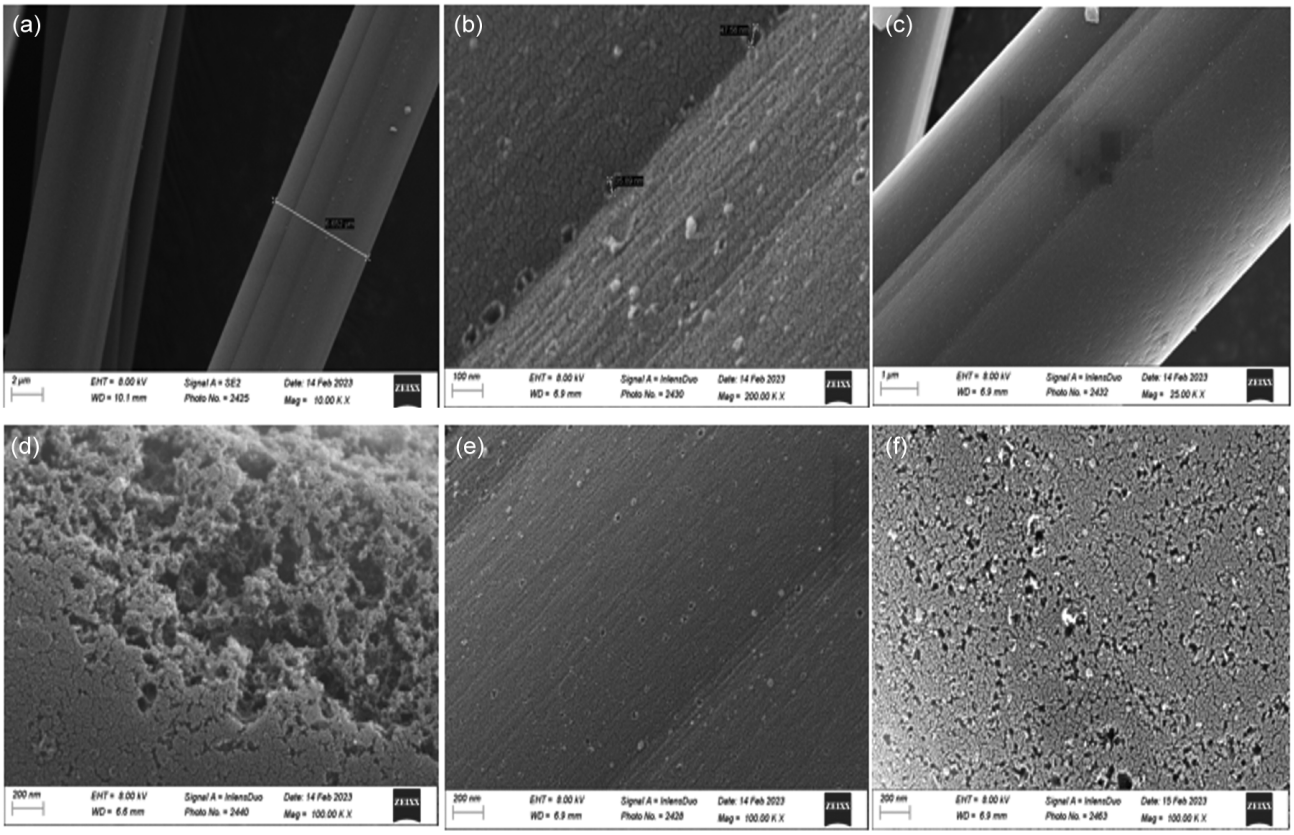

Fig. 5 — FESEM image of (a) Carbonized Rayon Fabric, (b) RSM-1, (c) RSM-1, (d) RSM-3, (e) RSM-5, and (f) RSM-7

cavities and cracks is visible on the fibre surface. The SEM images also coincide with the test results in Table 1, indicating a controlled reaction of CO_2 with the carbon fibre surface, resulting in a moderate surface area and pore-size distribution with moderate strength.

3.6 X-Ray Diffraction Analysis (XRD)

X-ray diffraction analysis of samples (Carbonized rayon, RSM-1, RSM-3, RSM-5 & RSM-7 was carried out using an X-ray diffractometer (XRD) (Make- Bruker, Model – D8 Advance). The analysis was done using Cu Ka radiation, with a scanning range of 10–70 (2θ). Fig. 6 describes the XRD pattern of carbonized rayon and activated carbon fabric RSM-1, RSM-3, RSM-5 & RSM-7, respectively.

XRD pattern of ACF shows a broadened peak with the absence of a sharp peak, revealing a predominantly amorphous structure[37]. Fig. 6 shows

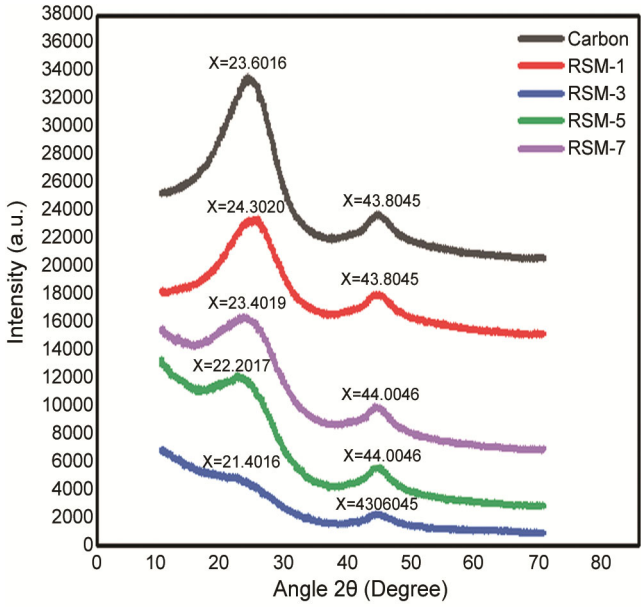

Fig. 6 — XRD pattern of Carbonized and Activated rayon fabric as (RSM-1, 3, 5 & 7)

that the typical amorphous structure in ACF is confirmed with two strong peaks at 2θ of ~23.6^0 and ~44^0, corresponding to the (002) and (101) crystal planes, respectively[38,39]. A similar nature is also observed for carbonized fabric. As described under section 3.1 Table 1, ACF samples were prepared under different conditions. Compared with carbonized rayon, the activated samples (RSM-1 to RSM-7) exhibit peak broadening and reduced intensity. Treatment of carbon fabric with CO_2 during the activation reaction enhances internal surface area and porosity under different conditions. Further, the amorphous nature of ACF increases with increasing BET surface area. This is well reflected in Fig. 6, where the peak broadens for the activated samples. However, carbonised rayon exhibits greater crystallographic plane formation, resulting in higher peak intensity.

3.7 Tensile and Bending Length Measurements

Tensile strength measurement on samples (Carbonized rayon, RSM-1, RSM-3, RSM-5 & RSM-7) was carried out on a 25 X 100 mm gauge length using a Universal Testing Machine (UTM) (Make – Dak System Inc's, Model – Series 9000). Tensile strength of ~ 80.5 kgf/cm^2 was obtained for carbonized rayon, which further decreased to ~57.5 kgf/cm^2(Sample RSM-1, surface area ~870 m^2/gm). Further, Table 2 shows that an increase in surface area has led to decreases in tensile strength, mass, and bending length. Also, the flexural rigidity of all representative samples was calculated as under

$$G = M \times C^3$$
$$= M \times C^3 \times 9.8 \times 10^{-6}$$

where G is the Flexural rigidity in μNm; M, Mass of sample in g/m^2 and C, Bending length in mm.

Flexural rigidity is also found to decrease with increasing surface area.

Table 2 — Comparative analysis of tensile strength, bending length, mass and flexural rigidity

S No.	Sample code	BET surface area, m^2/g	Tensile Strength, kgf/cm^2	Bending length, mm	Mass, g/m^2	Flexural Rigidity, μNm
01	Carbonized rayon	14.0	80.5	23	320	38.155
02	RSM-1	870.32	57.5	21	285	25.865
03	RSM-3	2533.33	19.5	18	120	6.858
04	RSM-5	1544.23	28.5	19	205	13.779
05	RSM-7	1318.76	51.3	20	220	17.248

4 Conclusion

Activated carbon fabric samples were prepared under a constant flow rate of activating gas and varying conditions of activation temperature and time. The samples were characterized for BET surface area, pore size distribution, adsorption isotherm, pore volume, FTIR, XRD, and FESEM. All the samples prepared showed well-developed porous structure and micro porosity as observed from the BET analysis. The porosity development in the samples is also evident from the surface roughness and visibility of small pits as observed by FESEM images. Further, peak broadening in XRD analysis of ACF samples confirmed an increase in amorphous content as compared to the carbonized fabric sample. This broadening of the peaks supports evidence of enhanced porosity development. Controlled porosity activated carbon with predominant microporosity (Pores < 20 Å) is desirable for the adsorption of gaseous contaminants. In view of the above, efforts have been made to prepare samples with a highly microporous nature and a narrow pore-size distribution (~17-24 Å), along with moderate strength. From experimental results and evaluation of properties, it is observed that temperature has a marked influence on the development of surface area and porosity in rayon carbon fabrics. The temperature effect is more pronounced than the activation duration effect at the same activation agent flow rate. A balance of properties in terms of surface area (1544.23 m^2/gm.), with total pore volume 0.71 cc/gm, including 0.56 cc/gm micro pore volume, and moderate strength is achieved under optimum conditions of time 4.0 h, temperature 900 ℃ & CO_2 gas flow rate of 100ml/min (sample RSM-5 with burn-off ~ 46 %). Further, it can be concluded that highly microporous activated carbon fabric can be prepared under suitable processing conditions & selection of an appropriate precursor. Due to its high microporosity, the prepared ACF is likely to be used for applications such as vapour-phase adsorption of hazardous chemicals and pollutants, thereby facilitating environmental cleanup. Further, it is concluded that an increase in surface area leads to a decrease in fabric properties such as bending length, mass, tensile strength, and flexural rigidity due to the development of internal porosity, which needs to be addressed for some critical applications. Apart from this, being reasonably strong, these materials may find use in chemical protective garments for military applications.

References

1 Mohan A V & Bhaarathidhurai D, *Int J Innov Sci Res Technol*, 5 (2020) 4.
2 Tripathi N K, Singh V V, Sathe M, Thakre V B & Singh B, *Defence Sci J*, 68 (2018) 83.
3 Fei-Yee Y, Ting L, Chee-Heong O, Radzali O & Fei-Yee, *Adv Mater Sci*, 36 (2014) 118.
4 Wang Y, Qiu H, Ayasrah M, *Materials (Basel)*, 16 (2023) 2612.
5 Mo B, Wang L, Li L, Han B, Xu G, Wang K, Z Hang, Ni Z, He X & Zhou W, *J Chem Eng Japan*, 56 (2023) 1.
6 Martins I M, Sampaio A G, Lima G M G, Oliveira e Campos Maria A C, Rodgher S, Rodrigues-Siqueli A C, Baldan M R, Marcuzzo J S & Koga-Ito Cristiane Y, *Front Environ Sci*, 10 (2023) 2296.
7 Rania A, Alireza H M, Yaman B, Zaher H, *J Chem Eng*, 410 (2021) 128412.
8 Ferreira J, Salgueiro T, Marcuzzo J, Arruda E, Ventura J, Oliveira J. *Batteries*, 9 (2023) 178.
9 Zhen L, Bangxing R, Haojie D, Huan H, Huiping D, Chun Z, Pu W & Dionysios D, *J Water Res*, 171 (2020) 115456.
10 Ma, Jun X, Cellulose, 20 (2013).
11 Soni K K, Mouli K C, Dalai A K, Adjaye J, *Microporous and Mesoporous Mat*, 152 (2012) 224.
12 Su C I, Zeng Z L, Peng C & Lu C H, *Fibers Polymers*, 13 (2012) 21.
13 Bhati S, Mahur J S, Dixit S & Choubey O N, *Bulletin Korean Chem Soc*, 34 (2013) 569.
14 Bhati S, Mahur J S, Dixit S & Chobey O N, *Carbon Letters*, 15 (2014) 45.
15 Zhu J, Shi B, Zhu J, Chen L, *Waste Manag Res, J Sust Cir Economy*, 27 (2009) 553.
16 Ma, Hoa & Ly, Hung & Ho, Van & Nguyen, Pham & Nguyen, Dat & Vo, Kieu & Dinh P, Tuan, *Vietnam Journal of Science and Technology*, 55 (2017).
17 *Singh A & Lal D, J App Pol Sci*, 115 (2010) 2409.
18 Khamkeaw A, Asavamongkolkul T, Perngyai T, Jongsomjit B & Phisalaphong M, *Molecules*, 25 (2020) 4063.
19 Prasad G, Singh B and Vijayaraghavan R, *Defence Sci J*, 58 (2008) 686.
20 Amaraweera S M, Gunathilake C A, Gunawardene O H P, Dassanayake R S, Cho E B, Du Y, *Nanomaterials (Basel)*, 13 (2023) 2050.
21 Tadda M A, Ahsan A, Shitu A, Elsergany M, Arunkumar T, Jose B, Razzaque M A, Daud N N N, *J Adv Civil Eng Practice & Res*, 2 (1) (2016) 7.
22 Mao N, *High Performance Textiles and Their Applications*, (U.K. Woodhead), 5 (2014) 91.
23 Martin R M, Mori D, Noble R D, Gin D L, *Ind Eng Chem Res*, 55 (2018) 6547.
24 Golmohammadi S, Sorayani S, Bafqi M S, Bagherzadeh R, Latifi M & Gorgi M, *J Ind Text*, 45 (2015) 467.
25 Lu A X, McEntee M, Browe M A, Hall M G, Decoste J B & Peterson G W, *ACS Appl Mater Interf*, 9 (2017) 13632.
26 Chen L, Bromberg L, Lee J A, Zhang H, Gibson H S, Gibson P, Walker J, Hammond P T, Hatton A & Rutledge G C, *Chem Mater*, 22 (2010) 1429.
27 Lin J, Zhao G, *Polymers*, 8 (2016) 369.
28 Ying Z, Huang L, Ji L, Li H, Liu X, Zhang C, Zhang J & Yi G, *Materials*, 14 (2021) 1754.

29 Kim K W, Lee H M, Kang S H & Kim B J, *Polymers*, 13 (2021) 3918.
30 Brunauer S, Emmett P H, Teller E, *J Am Chem Soc*, 60 (1938) 309.
31 Jia Z, Pan J & Yuan D, *Chem Open*, 6 (2017) 554.
32 Wang S, Burgos F V, Furuse A, Yoshikawa Y, Tanaka H & Kaneko K, *Carbon*, 175 (2021) 77.
33 Viisanen Y, Lbadaoui-Darvas M, Alvarez Piedehierro A, Welti A, Nenes A & Laaksonen A *Langmuir, 40 (*2024**)** 20311.
34 Smith B C, *Spectroscopy*, 32 (2017) 14.
35 Gao H, Wang S, Hao M, Shao W, Zhang L & Ren X, *Energies*, 16 (2023) 3872.
36 Prasad A G D, Kumar J K & Sharanappa P, *Romanian J of Biophysics*, 21 (2011) 221.
37 Omri A & Benzina M, *Journal de la Société Chimique de Tunisie*, 14 (2012) 175.
38 Liu Q, Yang H Y & Tong LL, *Trans Nonferrous Met Soc China*, 24 (2014) 1905.
39 Li Z Q, Lu C J, Xia Z P, Zhou Y & Luo Z, *Carbon*, 45 (2007) 1686.